



The formation of NeH^+ in static vacuum mass spectrometers and re-determination of $^{21}\text{Ne}/^{20}\text{Ne}$ of air

Domokos Györe^{a,*}, Andrew Tait^a, Doug Hamilton^b, Finlay M. Stuart^a

^a Isotope Geosciences Unit, Scottish Universities Environmental Research Centre (SUERC), East Kilbride G75 0QF, UK

^b Thermo Fisher Scientific, Hanna-Kunath-Straße 11, 28199 Bremen, Germany

Received 3 April 2019; accepted in revised form 31 July 2019; Available online 7 August 2019

Abstract

Air-derived neon is used for routine calibration of magnetic sector mass spectrometers, principally for determining sensitivity and mass discrimination for Ne isotope determinations. The commonly accepted $^{21}\text{Ne}/^{20}\text{Ne}$ ratio of air (0.002959 ± 0.000022 ; Eberhardt et al. (1965) does not take account of the contribution of $^{20}\text{NeH}^+$ at $m/z = 21$. Honda et al. (2015) and Wielandt and Storey (2019) have recently re-determined the $^{21}\text{Ne}/^{20}\text{Ne}_{\text{air}}$ by resolving $^{20}\text{NeH}^+$ from $^{21}\text{Ne}^+$. The $^{21}\text{Ne}/^{20}\text{Ne}_{\text{air}}$ values of the two studies differ by 1.8%, beyond the uncertainty of the measurements ($\pm <0.1\%$). We have developed a protocol for precise determination of NeH^+ in air using a low-resolution Thermo Fisher ARGUS VI mass spectrometer and use it to re-determine the $^{21}\text{Ne}/^{20}\text{Ne}$ of air. $^{22}\text{NeH}^+ / ^{22}\text{Ne}^+$ measured at different H_2^+ and Ne^+ intensities reveal that (i) the partial pressure of H_2^+ in the instrument is the primary control on NeH^+ production, and (ii) increasing Ne^+ pressure suppresses the formation of NeH^+ . Calibration curves of $^{22}\text{NeH}^+ / ^{22}\text{Ne}^+$ vs. $^{22}\text{Ne}^+$ at constant H_2^+ are used to calculate the $^{20}\text{NeH}^+$ production in aliquots of air-derived Ne and allow for hydride correction at $m/z = 21$. The fully isobaric interference-corrected Ne isotope compositions measured at different electron energy (eV) settings define a single mass fractionation line in $^{22}\text{Ne}/^{20}\text{Ne}$ vs. $^{21}\text{Ne}/^{20}\text{Ne}$ space. The $^{20}\text{NeH}^+ / ^{21}\text{Ne}^+$ ratio varies between 0.4% (90 eV) and 2.3% (60 and 70 eV). Correcting for $^{20}\text{NeH}^+$ assuming $^{22}\text{NeH}^+ / ^{20}\text{NeH}^+ = ^{22}\text{Ne}/^{20}\text{Ne}$ yields an over-correction of up to 0.7% and the data do not plot on a single mass fractionation line. Our study defines $^{21}\text{Ne}/^{20}\text{Ne}_{\text{air}}$ to be $0.002959 \pm 0.14\%$ (1σ) assuming $^{22}\text{Ne}/^{20}\text{Ne} = 0.102$ (Eberhardt et al., 1965). This overlaps the value determined by Wielandt and Storey (2019), albeit with a slightly higher uncertainty. However, our value is statistically more robust and accounts for the dependency on hydride formation by Ne partial pressure. From this we conclude that high precision Ne isotope ratio determinations in future require the quantification of $^{20}\text{NeH}^+$. The improved precision of air $^{21}\text{Ne}/^{20}\text{Ne}$ will result in more precise cosmogenic ^{21}Ne surface exposure and (U + Th)/Ne ages.

© 2019 Elsevier Ltd. All rights reserved.

Keywords: Noble gas mass spectrometry; ARGUS VI mass spectrometer; Multi-collection; Ne isotopic ratio; Low resolution; Hydride (NeH) correction; Cosmogenic; Radiogenic dating

1. INTRODUCTION

The precise determination of the noble gas isotopic composition of air is essential because it is routinely used to cal-

ibrate magnetic sector mass spectrometers. Further, variable amounts of air-derived noble gases are present in all terrestrial and extra-terrestrial material that can obscure the intrinsic isotopic composition and contribute significantly to the uncertainty of the corrected isotopic composition. The precise determination of the isotopic composition of noble gases in air is essential for many applications.

* Corresponding author.

E-mail address: Domokos.Gyore@glasgow.ac.uk (D. Györe).

Recent advances in magnetic sector mass spectrometry have led to increased precision and accuracy of He, Ne and Ar isotopic ratio determinations that have been exploited to refine air compositions (Honda et al., 2015; Mark et al., 2011; Mishima et al., 2019; Wielandt and Storey, 2019).

All three Ne isotopes (20 , 21 , 22 Ne) are primordial in origin, and are produced by nuclear processes in nature, making it an exceptional geochemical tracer. The Ne isotopic composition of meteorites and lunar regolith material have been key to identifying distinct primordial components of the early solar system history and determining how the planets formed (Black, 1972; Wieler, 2002). Neon isotopes in samples of terrestrial mantle have allowed the origin of Earth's volatile inventory to be determined and have revealed how the interior has evolved since accretion (Colin et al., 2015; Harrison et al., 1999; Moreira et al., 1998). The Ne isotope composition of crustal fluids can be used to quantify the contribution of magmatic volatiles and to trace fluid interaction histories (Ballentine et al., 2005; Ballentine and O'Nions, 1991). Cosmogenic 21 Ne produced in rocks in the upper few centimeters of Earth surface is now widely used to unravel long-term landscape development, particularly in arid regions that are sensitive to climate change (Ma and Stuart, 2018). The recently developed (U + Th)/ 21 Ne chronometer is finding use for determining the timing of Earth processes that have hitherto proved difficult to date (Gautheron et al., 2006).

The majority of the historical measurements of the Ne isotope composition of air (Bottomley et al., 1984; Eberhardt et al., 1965; Heber et al., 2009; Nier, 1950; Valkiers et al., 1994; Walton and Cameron, 1966) have not accounted for the effect of $^{20}\text{NeH}^+$ at $^{21}\text{Ne}^+$ as the resolving power of most instruments have not allowed the two peaks to be separated ($m/\Delta m = 3271$; Table 1). Consequently, the $^{21}\text{Ne}/^{20}\text{Ne}$ ratio of the global reference material may be over-estimated. New high-resolution mass spectrometers that allow the neon hydride ($^{20}\text{NeH}^+$) peak to be adequately separated from $^{21}\text{Ne}^+$ have permitted more accurate and precise determinations of air $^{21}\text{Ne}/^{20}\text{Ne}$ ratio

(Honda et al., 2015; Wielandt and Storey, 2019) (Fig. 1). Honda et al. (2015) re-determined the $^{21}\text{Ne}/^{20}\text{Ne}_{\text{air}}$ to be 0.002905 ± 0.000003 (1σ), for an assumed $^{22}\text{Ne}/^{20}\text{Ne}$ of 0.102 ± 0.0008 (Eberhardt et al. 1965). This is significantly lower than the widely-used value of Eberhardt et al. (1965) (0.002959 ± 0.000022 , 1σ), and a more recent high precision determination (0.0029577 ± 0.0000007) by Wielandt and Storey (2019). The reason for the 1.8% difference between the new values is currently unresolved but it places significant limitations on the routine geoscience applications of Ne isotopes.

Neither of the recent studies investigated the extent of, or controls on, NeH^+ formation in static vacuum mass spectrometers. This is important as the majority of magnetic sector mass spectrometers currently used for noble gas isotope determinations do not have the ability to resolve the $^{20}\text{NeH}^+$ and $^{21}\text{Ne}^+$ peaks. Where $^{20}\text{NeH}^+$ corrections have been made at low resolution, they are based on the measured $^{22}\text{NeH}^+$ beam intensity and assumption that $^{22}\text{NeH}^+ / ^{20}\text{NeH}^+ = ^{22}\text{Ne} / ^{20}\text{Ne}$ (Codilean et al., 2008; Poreda and di Brozolo, 1984; Wielandt and Storey, 2019). However, analysis of Ne^+ vs. NeH^+ data of Honda et al. (2015) and Wielandt and Storey (2019), suggests that NeH^+ formation is independent of the partial pressure of Ne^+ , thus the simple correction technique needs to be refined.

Here we present a series of experiments aimed at determining how NeH^+ is formed in a low-resolution static vacuum mass spectrometer with a standard Nier-type ion source (Thermo Fisher ARGUS VI). We have developed a protocol to quantify the production of $^{20}\text{NeH}^+$ on the basis of the measured $^{22}\text{NeH}^+$. Using neon isotope determinations of large volumes of air, in a manner similar to the procedure we have used previously to determine the Ar isotopic composition of air (Mark et al. 2011), has allowed a re-determination of the air $^{21}\text{Ne}/^{20}\text{Ne}$ value. Further, we consider how the precise NeH^+ correction is unavoidable for routine application of Ne isotope geochemistry.

Table 1
Potential isobaric interferences occurring at Ne compounds relevant in this study.

Ne compound	Interference	Mass (g/mol)	$m/\Delta m$
$^{20}\text{Ne}^+$ M = 19.992440 g/mol	$^{40}\text{Ar}^{2+}$	19.981190	1777
	H^{19}F^+	20.006228	1450
	$\text{H}_2^{18}\text{O}^+$	20.014810	894
	$\text{C}_3\text{H}_4^{2+}$	20.015650	861
$^{21}\text{Ne}^+$ M = 20.993847 g/mol	$^{63}\text{Cu}^{3+}$	20.976534	1213
	$^{20}\text{NeH}^+$	21.000265	3271
	$^{12}\text{CH}_2^{12}\text{C}^{16}\text{O}^{2+}$	21.005283	1836
	$^{12}\text{C}_3\text{H}_6^{2+}$	21.023475	709
	$^{12}\text{C}_3\text{H}_6^{*2+}$	21.020933	775 ^a
$^{22}\text{Ne}^+$ M = 21.991386 g/mol	$^{12}\text{C}^{16}\text{O}^{16}\text{O}^{2+}$	21.994915	6232
	$^{12}\text{C}^{18}\text{O}^{16}\text{O}^{2+}$	22.997038	10,582
$^{22}\text{NeH}^+$ M = 22.999211 g/mol	$^{13}\text{C}^{17}\text{O}^{16}\text{O}^{2+}$	22.998701	45,096
	$^{12}\text{C}_2\text{H}_5\text{OH}^{2+}$	23.020933	1059

^a Acetone fragment, elimination of oxygen from $\text{H}_3\text{C-CO-CH}_3$ molecule.

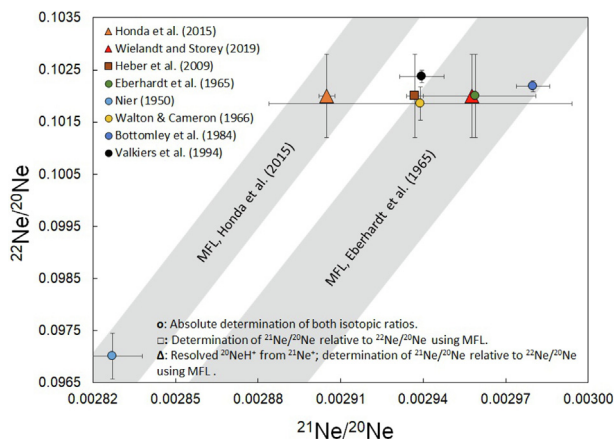


Fig. 1. Previous determinations of the Ne isotopic composition of air. With the exception of [Honda et al. \(2015\)](#) and [Wielandt and Storey \(2019\)](#) all studies have assumed $m/z = 21$ represents ^{21}Ne peak rather than correcting for the presence of $^{20}\text{NeH}^+$. MFL: Mass fractionation line, following square root law. Uncertainties shown are 1σ . The uncertainty of the [Wielandt and Storey \(2019\)](#) air value is smaller than symbol.

2. ANALYTICAL PROCEDURE

The data reported in this study are derived from the analysis of aliquots of $\sim 2.2 \times 10^{-8} \text{ cm}^3$ STP of Ne, extracted from a 2 litre air reservoir at $\sim 1390 \text{ Pa}$ and purified in an all-metal system maintained at ultra-high vacuum using a combination of turbo-molecular and triode ion pumps. Active gases are first removed from the air by exposure to a GP50 ZrAl alloy getter (SAES) held at 250°C for 15 min. The gas is then exposed to liquid nitrogen-cooled (-196°C) charcoal for 15 minutes to adsorb Ar, Kr & Xe. The remaining gas is exposed to charcoal at -243°C for 20 min using a Sumitomo coldhead (IceOxford) for 20 min to adsorb Ne. The residual He is pumped from the extraction line and cryopump volume, prior to the release of the Ne into the gas phase at -173°C . The Ne is equilibrated with the mass spectrometer for 45 seconds prior to analysis. The procedure for purification and cryogenic separation of Ne is fully automated. A GP50 ZrAl alloy getter held at room temperature and a liquid nitrogen-cooled charcoal finger have been installed on the source block of the mass spectrometer to reduce the levels of H, CO_2 and Ar during Ne isotope analysis. The liquid nitrogen-cooled charcoal trap on the line and mass spectrometer are fully automated, permitting non-stop operation for up to 80 h.

The Thermo Fisher ARGUS VI mass spectrometer used in this study is fitted with five Faraday cups (H2, H1, Axial, L1, L2) and a compact discrete dynode (CDD) electron multiplier at the L3 position. Whilst it is primarily used for multi-collector Ar isotope analysis by geochronology communities (e.g. [Bai et al., 2018](#)) flexible collector array allows multi-collection Kr and Xe isotope analysis ([Ruzie-Hamilton et al., 2016](#)) and by tuning the magnet position and the individual deflection voltages on the detectors neon peak coincidence can be achieved: $^{22}\text{Ne}^+$ on H2, $^{21}\text{Ne}^+$ on

Axial, $^{20}\text{Ne}^+$ on L2 detector ([Fig. 2](#)). Multi-collection provides a large time saving and increases the precision at the cost of the need of thorough and robust detector cross calibration. All the Faraday channels are equipped with $10^{12} \Omega$ amplifiers. The ion source has been tuned for maximum sensitivity using $^{20}\text{Ne}^+$ on the L2 detector. Prior to the experiments reported here the instrument sensitivity at 110 eV was determined to be $1.41 \times 10^{15} \text{ cps/cm}^3 \text{ STP } ^{20}\text{Ne}$ ($1 \text{ cps} = 1.6 \times 10^{-19} \text{ A}$). This is slightly lower than the ^{40}Ar sensitivity of $5 \times 10^{15} \text{ cps/cm}^3 \text{ STP}$ at 110 eV of a similar instrument reported by [Ruzie-Hamilton et al. \(2016\)](#).

The Faraday detectors were cross-calibrated using gain calibration electronics intrinsic to the Qtegra software. We also cross-calibrated the detectors by peak jumping of $m/z = 22$ on all the Faraday detectors for fixed source conditions. There was no measurable difference in the cross-calibration parameters determined by both techniques thus we used electronic gain calibrations. The CDD detector was cross-calibrated relative to the L2 Faraday cup by peak jumping the $m/z = 22$ beam on both detectors prior to analysis. This was monitored during all air analyses by measuring the $m/z = 21$ beam on the CDD and the axial Faraday. The cross-calibration factor did not change over the 4 months of analytical period.

No measurable Ne was present in all blank determinations. Beam intensities at $m/z = 20$ and $m/z = 22$ are due to the presence of $^{40}\text{Ar}^{2+}$ and CO_2^{2+} respectively (see [Section 3](#)). The peak at mass 21 in full procedure blanks was typically between 0.1 and 0.3‰ of the beam intensity in the air Ne measurements. This is neither $^{20}\text{NeH}^+$ nor $^{63}\text{Cu}^{3+}$, based on the absence of measurable $^{63}\text{Cu}^{3+}$ ($m/z = 21.67$) ([Codilean et al., 2008](#)). It is likely to be produced by organic compounds such as diketene ($^{12}\text{CH}_2^{12}\text{C}^{16}\text{O}^{2+}$), propene ($^{12}\text{C}_3\text{H}_6^{2+}$) or acetone fragment of $\text{CH}_3\text{CCH}_3^{*2+}$ ([Table 1](#)). The peak at $m/z = 23$ in blank determinations is 50–90% of that measured in air Ne analyses. Less than 5% of this is from $^{46}\text{CO}_2^{2+}$, thus it is also likely to be an organic compound such as ethanol ($\text{C}_2\text{H}_5\text{OH}^{2+}$).

3. ISOBARIC INTERFERENCES

The low resolution (<200) of the ARGUS VI mass spectrometer means that the Ne isotope peaks cannot be separated from the common isobaric interferences ([Table 1](#)). Separation of the $^{22}\text{Ne}^+$ peak from $^{12}\text{C}^{16}\text{O}_2^{2+}$ requires a resolution of 6232 ([Table 1](#)), which is unattainable with most magnetic sector mass spectrometers. In this study we have used the established protocol of determining the $^{12}\text{C}^{16}\text{O}_2^+/^{12}\text{C}^{16}\text{O}_2^{2+}$ for each measurement setting before analysis and using this factor along with $^{12}\text{C}^{16}\text{O}_2^+$ measured during each air Ne analysis (e.g. [Osawa, 2004](#)). $^{12}\text{C}^{16}\text{O}_2^+/^{12}\text{C}^{16}\text{O}_2^{2+}$ is determined in dynamic mode by peak jumping the $m/z = 44$ and 22 beams on the CDD at different electron energy settings. The $^{12}\text{C}^{16}\text{O}_2^+/^{12}\text{C}^{16}\text{O}_2^{2+}$ ratio decreases with increase in electron energy from 84.9 ± 1.3 at 60 eV to 42.0 ± 0.8 at 110 eV, with a plateau between 70 and 90 eV at the value of ~ 62 , consistent with previous studies (e.g. [King and Price, 2008](#)). We also determined $\text{CO}_2^+/\text{CO}_2^{2+}$ by measuring the beam intensity at $m/$

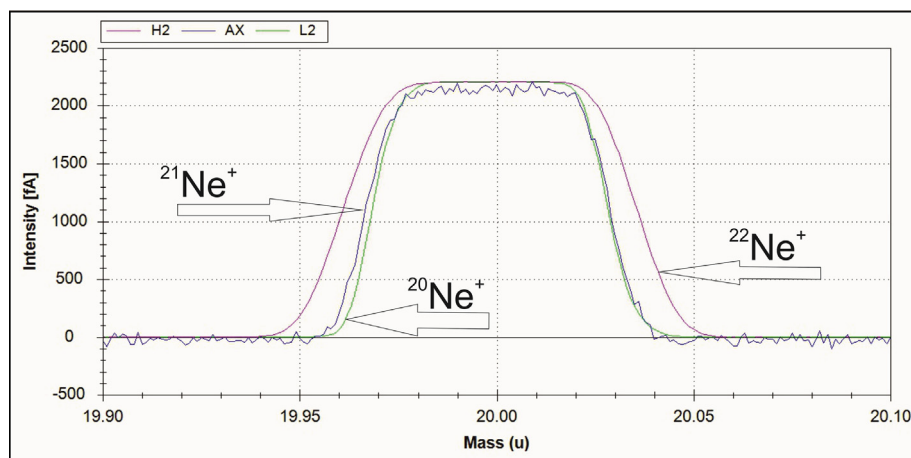


Fig. 2. The full peak coincidence of Ne isotopes measured by the Thermo Fisher ARGUS VI mass spectrometer at SUERC. Peak coincidence has been obtained between H2 ($^{22}\text{Ne}^+$), Axial ($^{21}\text{Ne}^+$) and L2 ($^{20}\text{Ne}^+$) Faraday detectors at magnetic field reference of 4.3224 V by changes to the position of the flight tube magnet and Faraday cup deflection voltages.

$z = 22.5$ ($^{13}\text{C}^{16}\text{O}^{16}\text{O}^{2+}$ and $^{12}\text{C}^{17}\text{O}^{16}\text{O}^{2+}$) and $m/z = 44$ ($^{44}\text{CO}_2^+$) in dynamic mode, and calculating the abundance of $^{45}\text{CO}_2^+$, where $(^{44}\text{CO}_2^+/^{45}\text{CO}_2^+)_{\text{natural}} = 83.86$. This confirms that the contribution of ^{22}Ne at mass 22 in dynamic mode is negligible. There is no statistical difference between $\text{CO}_2^+/\text{CO}_2^{2+}$ determined both ways. The $m/z = 45/22.5$ technique allows $\text{CO}_2^+/\text{CO}_2^{2+}$ ratio determination at Ne partial pressures that are representative of conditions of Ne isotope ratio analysis of air in this study. We found no significant differences in the $\text{CO}_2^+/\text{CO}_2^{2+}$ ratio by varying the H_2^+ and Ne^+ partial pressure (see e.g. [Niedermann et al., 1993](#)). The contribution of CO_2 at $m/z = 22$ determined by the measurement of $^{44}\text{CO}_2^+$ during air analysis and the pre-determined $\text{CO}_2^+/\text{CO}_2^{2+}$ is $< 0.3\%$.

In order to determine the $^{40}\text{Ar}^{2+}$ at $m/z = 20$ ($^{20}\text{Ne}^+$), $^{40}\text{Ar}^+$ was measured during Ne isotope ratio analysis and correction made using $^{40}\text{Ar}^+/^{40}\text{Ar}^{2+}$ ratios determined in dynamic mode by peak jumping of $m/z = 20$ and 40 on the CDD detector. $^{40}\text{Ar}^+/^{40}\text{Ar}^{2+}$ decreases from 3.6 ± 0.1 (60 eV) to 1.9 ± 0.1 (110 eV) with a plateau between 80 and 90 eV at 2.3 ± 0.1 , consistent with previous work ([Man et al., 1993](#)). It does not appear to be affected by H_2^+ partial pressure in the mass spectrometer. A linear correlation between $^{40}\text{Ar}^+/^{40}\text{Ar}^{2+}$ and $\text{CO}_2^+/\text{CO}_2^{2+}$ ($R^2 = 0.92$) is similar to that reported by [Balco and Shuster \(2009\)](#). Thus, we rule out strong source pressure dependency on $^{40}\text{Ar}^{2+}$ production and we use the Ar^{2+} generated in dynamic mode. The $^{40}\text{Ar}^{2+}$ contribution at $m/z = 20$ during the air Ne measurements is $< 0.2\%$.

The contribution of $\text{H}_2^{18}\text{O}^+$ at $m/z = 20$ is determined from the measured $\text{H}_2^{16}\text{O}^+$ and $(^{18}\text{O}/^{16}\text{O})_{\text{natural}} = 498.8$ and is $< 0.01\%$. Correction for H^{19}F^+ at $m/z = 20$ is based on the measurement of $^{19}\text{F}^+$ (typically 0.6 cps). In the worst case scenario where $m/z = 19$ is $^{19}\text{F}^+$, free from the interference of $\text{H}_2^{17}\text{O}^+$ and H^{18}O^+ fragment, and $\text{F}^+ = \text{H}^{19}\text{F}^+$ we calculate the H^{19}F^+ contribution at $m/z = 20$ to be $< 0.02\%$. Organic compounds ([Table 1](#)) are maintained at low levels (~ 0.001 fA) by baking the mass spectrometer at 350 °C.

4. DISCUSSION

4.1. the formation of NeH^+

[Honda et al. \(2015\)](#) and [Wielandt and Storey \(2019\)](#) determined levels of $^{20}\text{NeH}^+$ that contributed $\sim 2\%$ of the peak at $m/z = 21$ in analyses of air-derived Ne. This suggests that high precision Ne isotopic analysis using low resolution instruments require routine determination of $^{20}\text{NeH}^+$. Neither study determined the controls on NeH^+ formation.

[Moran and Friedman \(1963\)](#) showed that the majority of NeH^+ generated in gas-source mass spectrometers occurs via two reactions:

- $\text{H}_2^+ + \text{Ne} = \text{NeH}^+ + \text{H}$, and
- $\text{H}_2 + \text{Ne}^+ = \text{NeH}^+ + \text{H}$.

We have measured the $^{22}\text{NeH}^+/^{22}\text{Ne}^+$ ratio in pipettes of constant amounts of air-derived Ne with varying H_2^+ levels in order to determine the importance of reaction path (a). The level of hydrogen in the mass spectrometer was adjusted by manually varying the degree of closure of source GP50 getter valve. H_2^+ and CO_2^+ were analysed at the beginning of each analysis sequence (7 min) allowing precise $^{22}\text{NeH}^+/^{22}\text{Ne}^+$ determinations to be made by peak jumping of mass 22 and 23 (2 h). In order to determine the importance of reaction path (b) these experiments were repeated with varying amounts of air-derived Ne, by taking multiple air shots from the reservoir, while keeping the H_2^+ level constant ([Table 2](#)).

$^{22}\text{NeH}^+/^{22}\text{Ne}^+$ increases systematically with increasing H_2^+ (at constant $^{22}\text{Ne}^+$) for all electron energy settings ([Fig. 3A](#)). This implies that reaction path (a) dominates because linearity between atomic hydrogen and H_2^+ cannot be assumed, as H_3^+ and other species are formed in the source (e.g. [Smyth, 1925](#); [Sessions et al., 2001](#)). Hydride formation is highest at 60 and 70 eV ($^{22}\text{NeH}^+/^{22}\text{Ne}^+ >$

Table 2

The degree of hydride formation expressed as $^{22}\text{NeH}^+ / ^{22}\text{Ne}^+$ in the ARGUS VI mass spectrometer with varying H_2^+ and Ne^+ concentrations at a number of different electron energy settings.

Electron energy (eV)	H_2^+ (fA)	$^{22}\text{Ne}^+$ (fA)	$^{22}\text{NeH}^+ / ^{22}\text{Ne}^+$ ($\times 10^{-6}$)	Electron energy (eV)	H_2^+ (fA)	$^{22}\text{Ne}^+$ (fA)	$^{22}\text{NeH}^+ / ^{22}\text{Ne}^+$ ($\times 10^{-6}$)
60	Varying amount of Ne^+ at constant H_2^+			70	Varying amount of Ne^+ at constant H_2^+		
	3.3 (1.2)	188.94 (0.04)	69.4 (0.5)		9.9 (0.1)	303.46 (0.03)	83.1 (3.0)
	3.5 (0.8)	190.45 (0.06)	69.9 (1.1)		9.5 (0.1)	301.18 (0.04)	86.4 (0.5)
	4.0 (0.3)	189.99 (0.10)	69.1 (1.3)		9.0 (0.3)	302.63 (0.21)	87.1 (7.4)
	3.8 (0.9)	PNF	N/A		9.6 (0.2)	1538.1 (0.9)	77.4 (1.9)
	3.4 (0.4)	PNF	N/A		9.8 (0.3)	1533.8 (0.3)	73.6 (2.9)
	4.1 (0.4)	975.4 (0.5)	PNF		PNF	PNF	N/A
	5.1 (1.1)	1988.8 (0.8)	PNF		PNF	PNF	N/A
	5.0 (0.7)	1970.6 (0.7)	70.2 (0.4)		11.3 (0.4)	3080.7 (1.1)	67.0 (1.2)
	4.4 (0.6)	1958.3 (0.8)	65.8 (0.4)		10.2 (0.2)	3078.4 (0.4)	64.8 (4.2)
	4.0 (0.6)	2956.3 (1.3)	60.7 (0.3)		9.4 (0.4)	4637.0 (1.3)	54.0 (0.4)
	4.4 (1.2)	2965.0 (1.2)	58.5 (0.3)		9.4 (0.2)	4643.7 (1.4)	53.6 (0.9)
	4.9 (0.7)	2950.5 (1.0)	56.8 (0.2)		PNF	PNF	N/A
	Varying amount of H_2^+ at constant Ne^+				Varying amount of H_2^+ at constant Ne^+		
	5.0 (0.1)	2175.9 (1.4)	56 (1)		8.5 (0.1)	2844.6 (1.3)	51 (1)
	4.7 (0.2)	2156.8 (0.5)	57 (1)		9.3 (0.3)	2843.1 (1.2)	47 (1)
	5.2 (0.2)	2152.5 (0.5)	56 (1)		9.2 (0.1)	2845.7 (1.5)	50 (2)
	9.8 (0.1)	2024.6 (0.6)	130 (4)		18.6 (0.1)	2905.3 (1.3)	97 (2)
	10.4 (0.1)	2039.5 (0.5)	117 (1)		17.9 (0.3)	2906.3 (1.2)	100 (1)
	10.0 (0.1)	2063.3 (0.7)	121 (2)		18.8 (0.1)	2932.7 (1.5)	97 (2)
16.8 (0.2)	2121.8 (1.2)	202 (3)	33.8 (0.2)	2841.7 (0.8)	168 (2)		
18.4 (0.3)	2052.4 (1.6)	205 (3)	33.6 (0.5)	2834.2 (0.8)	167 (3)		
18.7 (0.3)	2057.5 (0.5)	211 (2)	32.9 (0.2)	2831.5 (1.4)	170 (3)		
80	Varying amount of Ne^+ at constant H_2^+			90	Varying amount of Ne^+ at constant H_2^+		
	8.5 (0.6)	292.0 (0.1)	35.4 (0.6)		5.0 (0.1)	363.6 (0.1)	20.1 (2.7)
	7.6 (0.4)	291.0 (0.2)	35.8 (0.4)		5.4 (0.2)	346.4 (0.1)	24.5 (11.0)
	8.1 (1.1)	292.0 (0.2)	36.7 (0.4)		5.4 (0.3)	344.9 (0.1)	20.8 (1.3)
	8.2 (0.5)	1471.4 (0.6)	32.9 (0.3)		3.7 (0.5)	1604.1 (0.4)	15.1 (0.2)
	7.8 (0.2)	1468.9 (0.5)	33.0 (0.2)		3.6 (0.5)	1603.0 (0.4)	14.8 (0.1)
	7.8 (0.4)	1474.0 (0.5)	31.9 (0.3)		3.9 (0.8)	1611.3 (0.7)	14.4 (0.2)
	8.1 (0.8)	2982.0 (1.7)	27.8 (0.2)		4.0 (0.5)	3243.1 (1.1)	12.9 (0.1)
	7.5 (1.1)	2974.8 (1.6)	28.1 (0.2)		4.9 (0.2)	3237.7 (1.1)	12.9 (0.1)
	6.2 (2.1)	2989.6 (1.1)	28.4 (0.2)		3.5 (0.9)	3233.3 (1.0)	12.7 (0.1)
	8.3 (0.8)	4552.9 (2.3)	23.9 (0.2)		3.8 (0.7)	4872.2 (1.8)	12.8 (0.1)
	9.1 (0.7)	4517.5 (1.3)	23.4 (0.2)		3.6 (0.9)	4882.4 (2.3)	13.4 (0.1)
	8.1 (0.3)	4557.0 (1.7)	23.0 (0.2)		3.8 (0.8)	4749.8 (2.4)	PNF
	Varying amount of H_2^+ at constant Ne^+				Varying amount of H_2^+ at constant Ne^+		
	9.3 (0.3)	3069.1 (1.3)	28 (1)		5.4 (0.3)	3199.7 (0.4)	16.0 (0.2)
	9.9 (0.2)	3068.3 (1.5)	26 (1)		5.0 (0.2)	3209.2 (0.9)	16.0 (0.2)
	9.5 (0.1)	3071.7 (1.6)	28 (1)		5.0 (0.1)	3195.2 (0.8)	15.6 (0.3)
	18.4 (0.4)	3187.6 (3.7)	49 (1)		10.6 (0.3)	3308.4 (1.0)	27.0 (0.6)
	19.0 (0.1)	3189.9 (2.8)	53 (1)		11.1 (0.2)	3326.3 (0.8)	27.5 (0.4)
	18.9 (0.2)	3176.2 (1.8)	54 (1)		PNF	3547.5 (1.0)	27.6 (0.3)
34.6 (0.2)	3088.2 (1.9)	81 (1)	17.8 (0.1)	3211.0 (0.7)	40.4 (0.5)		
34.3 (0.2)	3096.2 (1.6)	82 (3)	18.7 (0.2)	3201.8 (0.5)	39.9 (0.4)		
33.0 (0.1)	3078.0 (2.2)	79 (1)	17.7 (0.3)	3211.3 (1.0)	40.5 (0.5)		
100	Varying amount of Ne^+ at constant H_2^+			110	Varying amount of Ne^+ at constant H_2^+		
	2.6 (0.9)	315.9 (1.0)	16.4 (0.4)		2.2 (0.5)	338.8 (0.9)	17.4 (0.3)
	1.9 (0.5)	314.3 (0.7)	16.1 (0.4)		2.4 (0.5)	341.3 (0.9)	16.8 (0.4)
	PNF	313.2 (0.7)	17.0 (0.5)		PNF	338.6 (1.0)	16.5 (0.4)
	2.5 (0.3)	1588.7 (3.3)	10.9 (0.2)		PNF	1709.6 (4.7)	12.7 (0.1)
	2.6 (0.9)	1581.7 (1.1)	14.7 (0.1)		PNF	1708.8 (4.7)	12.6 (0.2)
	2.2 (0.4)	1577.5 (2.1)	13.6 (0.1)		3.3 (0.5)	1716.4 (4.6)	12.8 (0.1)
	2.0 (0.6)	3171.1 (5.4)	12.3 (0.1)		2.7 (0.8)	3425.3 (6.5)	12.0 (0.1)
	2.4 (0.5)	3183.0 (6.0)	11.9 (0.1)		2.2 (0.7)	3449.6 (7.8)	11.9 (0.1)
	2.5 (0.9)	3195.3 (5.9)	11.7 (0.1)		3.0 (0.2)	3431.6 (7.7)	11.9 (0.1)
	2.1 (0.9)	4791.2 (8.6)	12.1 (0.1)		2.6 (0.5)	5124.9 (12.3)	12.0 (0.1)
	1.6 (0.5)	4795.0 (10.5)	12.2 (0.1)		2.2 (0.4)	5158.3 (8.7)	11.9 (0.1)
	2.4 (1.0)	4769.5 (8.7)	12.2 (0.1)		PNF	5082.2 (2.5)	12.5 (0.1)

(continued on next page)

Table 2 (continued)

Electron energy (eV)	H ₂ ⁺ (fA)	²² Ne ⁺ (fA)	²² NeH ⁺ / ²² Ne ⁺ (× 10 ⁻⁶)	Electron energy (eV)	H ₂ ⁺ (fA)	²² Ne ⁺ (fA)	²² NeH ⁺ / ²² Ne ⁺ (× 10 ⁻⁶)
Varying amount of H ₂ ⁺ at constant Ne ⁺				Varying amount of H ₂ ⁺ at constant Ne ⁺			
	2.7 (0.1)	3496.1 (2.1)	12.2 (0.7)		4.0 (0.2)	3573.7 (5.4)	11.6 (0.4)
	3.5 (0.3)	3428.6 (4.1)	12.1 (0.5)		3.7 (0.3)	3578.0 (7.1)	12.0 (0.4)
	3.0 (0.1)	3439.3 (6.3)	11.4 (0.6)		3.6 (0.2)	3584.4 (8.6)	11.8 (0.4)
	8.9 (0.1)	3266.9 (4.9)	26.3 (1.1)		8.7 (0.3)	3568.2 (2.5)	24.9 (0.8)
	8.2 (0.2)	3293.2 (1.7)	24.3 (0.4)		8.7 (0.3)	3581.8 (2.5)	21.6 (0.5)
	PNF	PNF	PNF		7.7 (0.3)	3577.6 (2.9)	21.3 (0.6)
	11.1 (0.1)	3238.3 (6.1)	31.8 (0.9)		13.6 (0.2)	3578.2 (15.2)	32.7 (0.7)
	10.4 (0.5)	3245.5 (3.9)	31.9 (0.8)		13.3 (0.4)	3519.2 (4.7)	33.3 (1.0)
	11.8 (0.2)	3250.2 (3.1)	32.0 (0.5)		13.2 (0.1)	3530.9 (9.7)	32.0 (0.7)

²²Ne⁺ is corrected for CO₂⁺ (see text). M/z = 23 (²²NeH⁺) is blank corrected.

1σ uncertainties are in brackets. At constant Ne⁺ 3 analysis at 3 settings, at constant H₂⁺ 3 analysis at 3 settings have been carried out.

PNF: Peak not found. N/A: Not applicable. Occasional high error on H₂⁺ measurements are due to peak-centering issues.

Data are plotted on Fig. 3A (constant ²²Ne⁺) and 3B (constant H₂⁺) using weighted (1/σ²) averages.

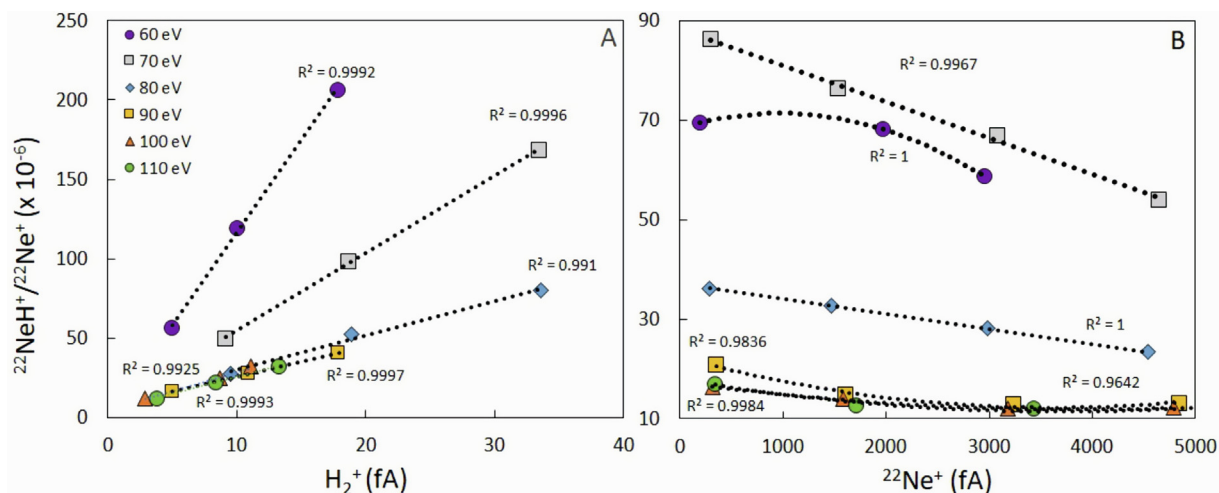


Fig. 3. (A) The degree of hydride formation with respect to H₂⁺ at constant Ne⁺, and (B) Ne⁺ and constant H₂⁺, at different electron energy settings in the ARGUS VI mass spectrometer. The strong positive correlation between ²²NeH⁺/²²Ne⁺ and H₂⁺ (A), regardless of the electron energy, proves that the chemical reaction H₂⁺ + Ne = NeH⁺ + H dominates. The lack of a positive correlation between ²²NeH⁺/²²Ne⁺ and ²²Ne⁺ (B) suggests that the H₂ + Ne⁺ = NeH⁺ + H reaction is significantly less important (see text for details). The negative correlation between ²²NeH⁺/²²Ne⁺ and ²²Ne⁺ (B) implies that NeH⁺ formation is suppressed by increasing Ne⁺. Beam intensities are given in fA as sensitivity is a function of electron energy. 1σ uncertainties are smaller than symbols.

50 ppm). Linear relationships imply that despite the large number of different products generated when ionizing hydrogen (Smyth, 1925) the dominant products are likely to be a mixture of H₂⁺, H⁺ and H. In contrast, the ²²NeH⁺ production rate shows no strong relationship with Ne⁺ availability in the source (Fig. 3B). Over a large ²²Ne⁺ partial pressure range there is a minor negative relationship between ²²NeH⁺ formation and Ne⁺ availability. The decrease is most pronounced at 60–80 eV, while at > 90 eV hydride formation rate is less dependent on ²²Ne⁺ availability.

The absence of a positive correlation between ²²NeH⁺ and ²²Ne⁺ rules out reaction path (b) as the dominant formation mechanism. This also rules out the importance of atomic Ne in reaction path (a) because of the linearity between Ne and Ne⁺. Together with the positive relationship in Fig. 3A

this strongly implies the H₂⁺ + Ne = NeH⁺ + H reaction is the key mechanism for Ne-hydride formation and is controlled by H₂⁺ instead of the combination of H₂⁺ and atomic Ne. This is consistent with the kinetic theory of NeH⁺ formation (Kaul et al., 1961; Moran and Friedman, 1963) and previous observations (Niedermann et al., 1993). It implies that maintaining H₂⁺ level constant during analyses keeps the NeH⁺ constant. The ²²NeH⁺/²²Ne⁺ vs. ²²Ne⁺ relationship (Fig. 3B) implies that there may be either a small pressure-dependent sensitivity or a decrease in the concentration of ²²NeH⁺, or a combination of both, that may also explain the deviation from linearity. It is important to note that the ²²NeH⁺ production shown in Fig. 3B has been determined for a range of ²²Ne⁺ that extends to equivalent to the ²⁰Ne⁺ amount used for the precise ratio determinations (Sections 4.2 and 4.3).

Table 3

Ne isotopic ratios of air from the ARGUS VI mass spectrometer in multi-collection mode and the significance on $^{20}\text{NeH}^+$ correction method.

Electron energy (eV)	$^{22}\text{Ne}/^{20}\text{Ne}^{(1)}$	Uncorrected ⁽²⁾		Corrected ⁽³⁾		Corrected ⁽⁴⁾		
		$^{21}\text{Ne}/^{20}\text{Ne}$	$^{21}\text{Ne}/^{20}\text{Ne}$	$^{20}\text{NeH}^+$	$^{20}\text{NeH}^+ / ^{21}\text{Ne}^+$	$^{21}\text{Ne}/^{20}\text{Ne}$	$^{20}\text{NeH}^+$	$^{20}\text{NeH}^+ / ^{21}\text{Ne}^+$
60	0.10308 (7)	0.003043 (4)	0.002973 (5)	0.1279 (58)	2.33%	0.002973 (4)	0.1281 (8)	2.34%
	0.10311 (4)	0.003040 (4)	0.002971 (5)	0.1279 (58)	2.34%	0.002970 (4)	0.1281 (8)	2.34%
	0.10310 (4)	0.003042 (5)	0.002973 (6)	0.1272 (58)	2.34%	0.002973 (5)	0.1273 (8)	2.34%
	0.10307 (5)	0.003043 (4)	0.002974 (5)	0.1281 (58)	2.33%	0.002974 (4)	0.1284 (8)	2.34%
	0.10294 (1)	0.003041 (3)	0.002975 (5)	0.1517 (73)	2.21%	0.002971 (3)	0.1603 (10)	2.34%
	0.10316 (3)	0.003043 (4)	0.002975 (5)	0.1424 (67)	2.27%	0.002973 (4)	0.1468 (9)	2.34%
BG	0.10308 (3)	0.003042 (5)	0.002975 (6)	0.1420 (66)	2.27%	0.002973 (5)	0.1463 (9)	2.34%
	0.10320	0.0030423	0.0029733			0.0029725		
Error.	0.00006	0.0000045	0.0000055			0.0000042		
Rel. error.	0.05%	0.15%	0.18%			0.14%		
70	0.10159 (6)	0.003020 (3)	0.002950 (3)	0.1833 (42)	2.35%	0.002933 (4)	0.2282 (58)	2.94%
	0.10164 (7)	0.003022 (4)	0.002953 (4)	0.1831 (42)	2.35%	0.002936 (5)	0.2279 (58)	2.94%
	0.10150 (7)	0.003018 (4)	0.002949 (4)	0.1833 (42)	2.35%	0.002932 (4)	0.2282 (58)	2.94%
	0.10153 (7)	0.003021 (3)	0.002952 (4)	0.1836 (42)	2.35%	0.002935 (4)	0.2287 (58)	2.94%
	0.10156 (6)	0.003024 (3)	0.002955 (3)	0.1829 (42)	2.35%	0.002938 (3)	0.2275 (58)	2.94%
	0.10164 (2)	0.003028 (2)	0.002961 (3)	0.1989 (48)	2.25%	0.002941 (3)	0.2576 (65)	2.93%
BG	0.10159 (9)	0.003036 (4)	0.002969 (5)	0.1986 (47)	2.24%	0.002950 (5)	0.2570 (65)	2.92%
	0.10156	0.0030211	0.0029517			0.0029348		
Error.	0.00008	0.0000039	0.0000044			0.0000049		
Rel. error.	0.08%	0.13%	0.15%			0.17%		
80	0.10258 (5)	0.002997 (2)	0.002968 (2)	0.0803 (9)	0.96%	0.002961 (2)	0.1024 (20)	1.22%
	0.10260 (9)	0.002998 (4)	0.002970 (4)	0.0806 (9)	0.95%	0.002962 (4)	0.1029 (20)	1.22%
	0.10255 (5)	0.002993 (3)	0.002967 (3)	0.0907 (11)	0.89%	0.002957 (3)	0.1239 (24)	1.22%
	0.10253 (4)	0.002994 (3)	0.002967 (3)	0.0905 (11)	0.89%	0.002957 (3)	0.1233 (24)	1.22%
	0.10254 (2)	0.002994 (4)	0.002968 (4)	0.0906 (11)	0.89%	0.002958 (4)	0.1235 (24)	1.22%
	0.10255 (2)	0.002993 (4)	0.002966 (4)	0.0904 (11)	0.89%	0.002957 (4)	0.1232 (24)	1.22%
BG	0.10255 (2)	0.002995 (3)	0.002968 (3)	0.0905 (11)	0.89%	0.002958 (3)	0.1234 (24)	1.22%
	0.10254	0.0029950	0.0029674			0.0029586		
Error.	0.00003	0.0000038	0.0000033			0.0000039		
Rel. error.	0.03%	0.13%	0.11%			0.13%		
90	0.10432 (6)	0.003008 (2)	0.002996 (2)	0.0404 (3)	0.43%	0.002988 (3)	0.0656 (65)	0.69%
	0.10447 (8)	0.003005 (3)	0.002993 (3)	0.0384 (3)	0.43%	0.002985 (4)	0.0618 (61)	0.70%
	0.10448 (9)	0.003007 (3)	0.002995 (3)	0.0384 (3)	0.43%	0.002987 (3)	0.0619 (61)	0.70%
	0.10448 (7)	0.003007 (3)	0.002994 (3)	0.0385 (3)	0.43%	0.002986 (4)	0.0620 (61)	0.70%
	0.10441 (6)	0.003009 (3)	0.002997 (3)	0.0390 (3)	0.43%	0.002989 (4)	0.0631 (62)	0.69%
	0.10441 (9)	0.003007 (3)	0.002994 (3)	0.0390 (3)	0.43%	0.002986 (4)	0.0630 (62)	0.70%
BG	0.10441 (5)	0.003009 (3)	0.002996 (3)	0.0389 (3)	0.43%	0.002988 (4)	0.0628 (62)	0.69%
	0.10443	0.0030074	0.0029951			0.0029871		
Error.	0.00009	0.0000030	0.0000032			0.0000039		
Rel. error.	0.09%	0.10%	0.11%			0.13%		
100	0.10552 (37)	0.003016 (11)	0.003004 (11)	0.0365 (9)	0.41%	0.003000 (11)	0.0489 (14)	0.55%
	0.10553 (10)	0.003021 (4)	0.003009 (4)	0.0383 (10)	0.40%	0.003005 (4)	0.0516 (15)	0.55%
	0.10556 (10)	0.003020 (5)	0.003008 (5)	0.0382 (10)	0.40%	0.003004 (5)	0.0515 (15)	0.55%
	0.10547 (10)	0.003020 (4)	0.003008 (4)	0.0380 (10)	0.41%	0.003003 (4)	0.0512 (15)	0.55%
	0.10533 (14)	0.003022 (5)	0.003009 (5)	0.0408 (11)	0.40%	0.003005 (5)	0.0554 (16)	0.55%
	0.10540 (12)	0.003017 (4)	0.003005 (4)	0.0388 (10)	0.40%	0.003001 (4)	0.0524 (15)	0.55%
BG	0.10538 (14)	0.003019 (6)	0.003007 (6)	0.0385 (10)	0.40%	0.003003 (6)	0.0520 (15)	0.55%
	0.10546	0.0030195	0.0030075			0.0030033		
Error.	0.00016	0.0000054	0.0000055			0.0000053		
Rel. error.	0.15%	0.18%	0.18%			0.13%		
110	0.10485 (14)	0.003017 (5)	0.003005 (5)	0.0382 (2)	0.39%	0.003000 (5)	0.0553 (15)	0.57%
	0.10483 (16)	0.003013 (5)	0.003001 (5)	0.0405 (2)	0.39%	0.002996 (5)	0.0589 (16)	0.57%
	0.10488 (7)	0.003013 (4)	0.003001 (4)	0.0403 (2)	0.39%	0.002996 (4)	0.0585 (16)	0.57%
	0.10495 (9)	0.003011 (5)	0.002999 (5)	0.0405 (2)	0.39%	0.002994 (5)	0.0589 (16)	0.57%
	0.10501 (13)	0.003013 (4)	0.003001 (4)	0.0404 (2)	0.39%	0.002996 (4)	0.0587 (16)	0.57%
	0.10489 (20)	0.003015 (6)	0.003003 (6)	0.0425 (3)	0.39%	0.002998 (6)	0.0619 (17)	0.57%

(continued on next page)

Table 3 (continued)

Electron energy (eV)	$^{22}\text{Ne}/^{20}\text{Ne}^{(1)}$	Uncorrected ⁽²⁾		Corrected ⁽³⁾		Corrected ⁽⁴⁾		
		$^{21}\text{Ne}/^{20}\text{Ne}$	$^{21}\text{Ne}/^{20}\text{Ne}$	$^{20}\text{NeH}^+$	$^{20}\text{NeH}^+ / ^{21}\text{Ne}^+$	$^{21}\text{Ne}/^{20}\text{Ne}$	$^{20}\text{NeH}^+$	$^{20}\text{NeH}^+ / ^{21}\text{Ne}^+$
	<i>0.10459</i> (15)	<i>0.003009</i> (6)	<i>0.002998</i> (6)	<i>0.0410</i> (2)	<i>0.39%</i>	<i>0.002992</i> (6)	<i>0.0596</i> (16)	<i>0.57%</i>
BG	0.10490	0.0030129	0.0030015			0.0029964		
Error.	0.00014	0.0000048	0.0000050			0.0000051		
Rel. error.	0.13%	0.16%	0.17%			0.17%		

Outliers are marked *Italics*.

BG: Best Gaussian fit to the probability density distribution. Error: 1σ , Rel. error: Relative error (%), 1σ .

(1) $^{22}\text{Ne}/^{20}\text{Ne}$ ratios corrected for Ar and CO_2 , other for other isobaric interferences (see text).

(2) $^{21}\text{Ne}/^{20}\text{Ne}$ ratios corrected for everything other than $^{20}\text{NeH}^+$.

(3) Corrected $^{21}\text{Ne}^+$ on the basis of $^{22}\text{NeH}^+ / ^{22}\text{Ne}^+$ vs. $^{22}\text{Ne}^+$ calibration curves (see text).

(4) Corrected $^{21}\text{Ne}^+$ on the basis of measured $^{22}\text{NeH}^+$ assuming $^{22}\text{NeH}^+ / ^{20}\text{NeH}^+ = ^{22}\text{Ne}/^{20}\text{Ne}$ (aka traditional way).

The strong dependency of NeH^+ formation with hydrogen and Ne^+ level is also observed in the study of [Wielandt and Storey \(2019\)](#). They made NeH^+ corrections at different hydrogen and Ne^+ intensities. The $^{20}\text{NeH}^+$ contribution in their study is highest (1.16%) with high hydrogen background levels. NeH^+ formation at low hydrogen levels is dependent on the intensity of Ne^+ . The $^{20}\text{NeH}^+$ contribution at $m/z = 21$ (0.65–0.85% at 40,000–25,000 fA $^{20}\text{Ne}^+$, respectively) is in line with the observed decrease of NeH^+ signal with increasing Ne^+ in this study.

4.2. Correcting for $^{20}\text{NeH}^+$

The Ne isotopic composition of air has been measured seven times at several electron energy settings (Table 3). Analysis starts with a measurement of H_2^+ , $^{44}\text{CO}_2^+$, $^{40}\text{Ar}^+$ (10 min), followed by multi-collection of $^{22}\text{Ne}^+$ (H2) – $^{21}\text{Ne}^+$ (Ax) – $^{20}\text{Ne}^+$ (L2) for ~3 h. This allows the magnet current to remain unchanged and generate high precision Ne isotope ratio measurements. Beam intensities are determined by extrapolation to inlet time and isobaric interference corrections are carried out using the pre-determined

$\text{CO}_2^+ / \text{CO}_2^{2+}$ and $^{40}\text{Ar}^+ / ^{40}\text{Ar}^{2+}$ ratios and $\text{Ne}^+ - \text{NeH}^+$ calibration curves. Uncertainties induced by these corrections have been propagated. All data are plotted in Fig. 4A. The different electron energy settings yield clearly distinct isotope ratio data. The key point to note is that the corrected data plot along a trend that is consistent with a single mass fractionation line. The data from the 70 eV analyses plot below the commonly accepted air $^{22}\text{Ne}/^{20}\text{Ne}$ value (0.102; [Eberhardt et al. 1965](#)) while data from all other source settings have higher $^{22}\text{Ne}/^{20}\text{Ne}$. The extent of the fractionation is likely a simple function of electron energy ([Honda et al., 2015](#)). The hydride correction is most significant at 60 and 70 eV, on average 2.3% of the $^{21}\text{Ne}^+$ beam. This drops to ~0.4% at 90 eV and beyond (Table 3).

The best Gaussian fit to the probability density distribution ([Kirkup, 2012](#)) and 1σ uncertainty of each data group are reported in Table 4 and Fig. 4B. The uncertainty of the $^{22}\text{Ne}/^{20}\text{Ne}$ data is at a minimum at 80 eV (0.03%) and increases with electron energy to maximum of 0.13% at 110 eV. This may reflect decreasing source stability at high eV settings. The uncertainty of the $^{21}\text{Ne}/^{20}\text{Ne}$ ratios is a minimum (0.11%) at 80 and 90 eV, increasing at lower

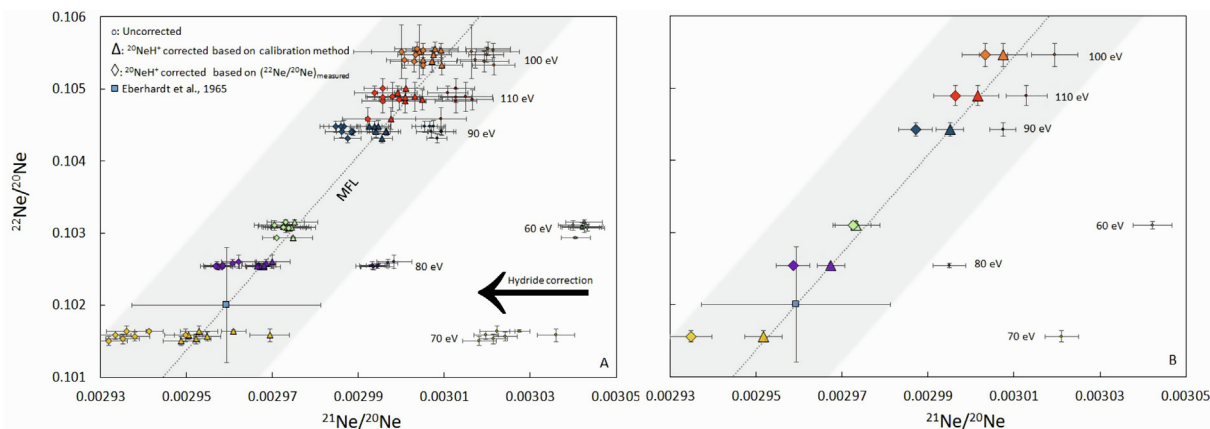


Fig. 4. Plots showing the effect of hydride correction to Ne isotope composition of air measured at different source electron energy settings (A). *Uncorrected* data (i.e. not corrected for $^{20}\text{NeH}^+$) display a large variation in $^{21}\text{Ne}/^{20}\text{Ne}$. The *corrected* data (see text) define a single mass fractionation line (MFL) while the data corrected using the measured $^{22}\text{NeH}^+ / ^{20}\text{NeH}^+ = ^{22}\text{Ne}/^{20}\text{Ne}$ does not define a single MFL and overestimate $^{20}\text{NeH}^+$ at all source conditions. The best Gaussian fit to the probability density distribution of each group (B) has a minimum uncertainty for $^{21}\text{Ne}/^{20}\text{Ne}$ at 80 & 90 eV (0.11%) and for $^{22}\text{Ne}/^{20}\text{Ne}$ at 80 eV (0.03%). All uncertainties are 1 sigma.

Table 4
Calculated $^{21}\text{Ne}/^{20}\text{Ne}$ composition of air.

Electron energy (eV)	$^{22}\text{Ne}/^{20}\text{Ne}$	$^{21}\text{Ne}/^{20}\text{Ne}^{(1)}$	$^{21}\text{Ne}/^{20}\text{Ne}^{(2)}$
60	0.10310 (6)	0.002973 (6)	0.002957 (6)
70	0.10156 (8)	0.002952 (4)	0.002958 (5)
80	0.10254 (3)	0.002967 (3)	0.002959 (3)
90	0.10443 (9)	0.002995 (3)	0.002959 (3)
100	<i>0.10546 (16)</i>	<i>0.003008 (6)</i>	<i>0.002955 (6)</i>
110	<i>0.10490 (14)</i>	<i>0.003002 (5)</i>	<i>0.002958 (5)</i>
BG (60–90 eV)			0.002959 (4)
rel. error			0.14%

$^{22}\text{Ne}/^{20}\text{Ne}$ values are that of Table 3.

BG: Best Gaussian fit to the probability density distribution. Error: 1σ , Rel. error: Relative error (%), 1σ . *Italics*: Not taken into account due to possible source instability.

⁽¹⁾: $^{21}\text{Ne}/^{20}\text{Ne}$ ratios corrected by Ne^+ - NeH^+ calibration curves.

⁽²⁾: $^{21}\text{Ne}/^{20}\text{Ne}$ ratios corrected for fractionation by Eq. (1) (see text), at the reference value of $^{22}\text{Ne}/^{20}\text{Ne} = 0.102$ and error is propagated accordingly. 1σ errors are shown as last significant figures in brackets.

Table 5
Recommendation for interference correction for Ne isotopes on the ARGUS VI low resolution mass spectrometer.

Compound	Interferes with	Pre-determine	Measure with Ne	Best approach
$^{44}\text{CO}_2^+$	$^{22}\text{Ne}^+$	$^{44}\text{CO}_2^+ / ^{44}\text{CO}_2^{2+}$ (44/22) and $^{45}\text{CO}_2^+ / ^{45}\text{CO}_2^{2+}$ (45/22.5) in dynamic mode and $^{45}\text{CO}_2^+ / ^{45}\text{CO}_2^{2+}$ in static mode f(H, Ne)	$^{44}\text{CO}_2^+$ (m/z = 44)	Optimize the ratio of Ne/interfering agent with Ne/NeH^+ formation
$^{40}\text{Ar}^{2+}$	$^{20}\text{Ne}^+$	$^{40}\text{Ar}^+ / ^{40}\text{Ar}^{2+}$ (40/20) in dynamic mode, evaluate pressure dependency (H, Ne) by correlation of $^{44}\text{CO}_2^+ / ^{44}\text{CO}_2^{2+}$	$^{40}\text{Ar}^{2+}$ (m/z = 40)	
$\text{H}_2^{18}\text{O}^+$ H^{19}F^+ $^{63}\text{Cu}^{3+}$ $^{20}\text{NeH}^+$	$^{21}\text{Ne}^+$	N/A	$\text{H}_2^{16}\text{O}^+$ (m/z = 18) F^+ (m/z = 19) $^{65}\text{Cu}^{3+}$ (m/z = 21.67) H_2^+ (m/z = 2), early in the sequence	Optimize ion source between stability and intensity of NeH^+ generation
$^{46}\text{CO}_2^+$	$^{22}\text{NeH}^+$	$\text{CO}_2^+ / \text{CO}_2^{2+}$ (see above)	$^{44}\text{CO}_2^+$ (m/z = 44)	N/A
Organics	$^{20,21}\text{Ne}$	blank	N/A	

electron energies due to increasing signal/noise ratio, and at higher electron energies, due to source instability.

The $^{21}\text{Ne}/^{20}\text{Ne}$ ratios corrected for $^{20}\text{NeH}^+$, assuming a direct linear relationship between $^{22}\text{NeH}^+$ and $^{20}\text{NeH}^+$ ($^{22}\text{NeH}^+ / ^{20}\text{NeH}^+ = ^{22}\text{Ne}/^{20}\text{Ne}$) (e.g. Wielandt and Storey, 2019), do not define a single mass fractionation line and appear to over-estimate the correction in all cases (Fig. 4). At 70 eV the corrected $^{21}\text{Ne}/^{20}\text{Ne}$ ratios differ by 0.7%, decreasing to $\sim 0.15\%$ at 100 and 110 eV. At 60 eV the difference is negligible, which is reflected in the shape of the $\text{NeH}^+ - \text{Ne}^+$ calibration curve (Fig. 3B). The differences in the two correction methods are significant relative to uncertainties at and below 90 eV. $^{21}\text{Ne}/^{20}\text{Ne}$ ratios that have been corrected using the two techniques overlap within uncertainty at 100 and 110 eV (Fig. 4B). Minimising the NeH^+ in the mass spectrometer may not be the best method for accurate and precise Ne isotope ratio measurements by low-resolution mass spectrometers because it may be associated with unexpected source instability (above

100 eV in our case). NeH^+ formation needs to be fully characterized in order to minimise the uncertainty of $^{21}\text{Ne}/^{20}\text{Ne}$. The nature of NeH^+ in the source is fundamentally different than any other interfering compound with Ne isotopes (CO_2 , Ar), which may require a high but quantifiable NeH^+ and optimum Ne^+/NeH^+ (Table 5).

4.3. The $^{21}\text{Ne}/^{20}\text{Ne}$ composition of air

Our hydride-corrected air data lie on a mass fractionation line in $^{22}\text{Ne}/^{20}\text{Ne} - ^{21}\text{Ne}/^{20}\text{Ne}$ space defined by:

$$\left[\frac{\sqrt{\frac{m_{20\text{Ne}}}{m_{22\text{Ne}}} - 1}}{\sqrt{\frac{m_{20\text{Ne}}}{m_{21\text{Ne}}} - 1}} \right] \left[\left(\frac{^{21}\text{Ne}}{^{20}\text{Ne}} \right)_{\text{measured}} - 1 \right] = \left[\frac{\left(\frac{^{22}\text{Ne}}{^{20}\text{Ne}} \right)_{\text{measured}}}{\left(\frac{^{22}\text{Ne}}{^{20}\text{Ne}} \right)_{\text{air}}} \right] - 1 \quad (1)$$

Applying this equation to calculate $^{21}\text{Ne}/^{20}\text{Ne}_{\text{air}}$ at the reference value of $^{22}\text{Ne}/^{20}\text{Ne}_{\text{air}} = 0.102$ (Eberhardt et al., 1965) at each electron energy setting we obtain $^{21}\text{Ne}/^{20}\text{Ne}$ ratios that vary between 0.002955 ± 0.000006 (100 eV) and 0.002959 ± 0.000003 (80 and 90 eV) (Table 4). The best Gaussian fit to the probability density distribution of the complete dataset yields $^{21}\text{Ne}/^{20}\text{Ne}_{\text{air}}$ of 0.002958 ± 0.000005 (0.15%, 1σ). Ignoring the data from 100 and 110 eV where source instability has affected data quality, the $^{21}\text{Ne}/^{20}\text{Ne}_{\text{air}}$ is 0.002959 ± 0.000004 (0.14%, at 1σ level). The degree of data scatter ($\pm 0.14\%$) and the mean analytical uncertainty ($\pm 0.13\%$) (obtained from 32 data points, 7 measurements at 4 different eV settings) are similar.

Our $^{21}\text{Ne}/^{20}\text{Ne}_{\text{air}}$ value overlaps with that determined by Wielandt and Storey (2019) and Eberhardt et al. (1965). It does not overlap with other determinations (Bottomley et al., 1984; Valkiers et al., 1994; Heber et al., 2009; Honda et al., 2015) apart from that of Walton and Cameron (1966) due to its high uncertainty in $^{21}\text{Ne}/^{20}\text{Ne}$ (1.9%, 1σ). The high $^{21}\text{Ne}/^{20}\text{Ne}_{\text{air}}$ determined by Bottomley et al. (1984) (0.002980 ± 0.000006) may be explained by the presence of NeH^+ , although they argue it is negligible. All other studies have produced significantly lower $^{21}\text{Ne}/^{20}\text{Ne}$ than our study (Fig. 5).

The uncertainty in the air $^{21}\text{Ne}/^{20}\text{Ne}$ determined here is a 5-fold improvement on the value ($\pm 0.74\%$, 1σ) determined by Eberhardt et al. (1965). It is less precise than the value published by Wielandt and Storey (2019) ($\pm 0.023\%$, 1σ). Based on the new understanding of NeH^+ production gained in this study it is likely that their uncertainty is significantly underestimated. The $^{20}\text{NeH}^+$ correction they used in low resolution mode was determined on the assumption that $^{22}\text{NeH}^+ / ^{20}\text{NeH}^+ = ^{22}\text{Ne} / ^{20}\text{Ne}$. We have shown this to be incorrect; NeH^+ production is inversely and non-linearly proportional to Ne^+ partial pressure.

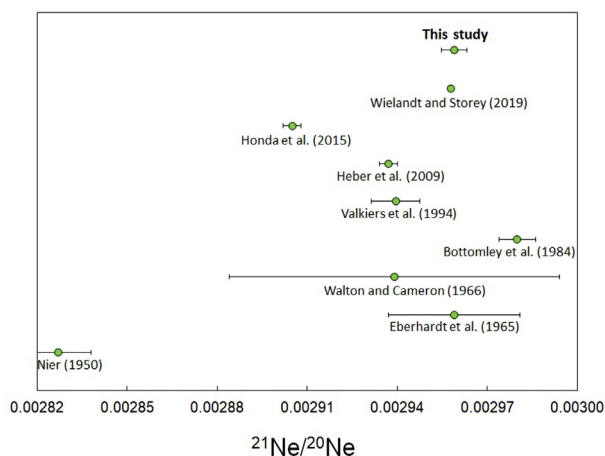


Fig. 5. $^{21}\text{Ne}/^{20}\text{Ne}$ composition of air. This study yields air $^{21}\text{Ne}/^{20}\text{Ne}$ of 0.002959 ± 0.000004 . This overlaps the Eberhardt et al. (1965) & Wielandt and Storey (2019) values, but no other moderately precise determinations. The uncertainty in the Wielandt and Storey (2019) $^{21}\text{Ne}/^{20}\text{Ne}$ value is underestimated (see text). 1 sigma uncertainty in case of Wielandt and Storey (2019) is smaller than symbol.

Consequently, the ‘dynamic’ dataset reported by Wielandt and Storey (2019) cannot be used in support of the ‘high intensity static data’. Thus, their whole static dataset ‘high and low intensity’ should be used. The best Gaussian fit to the probability density distribution of this dataset yields a significantly increased uncertainty ($\pm 0.1\%$, 1σ). Further, the intensity (pressure) effect on $^{21}\text{Ne}/^{20}\text{Ne}$ remains unresolved, suggesting that above uncertainty is a minimum. Thus, until a more thorough determination of $^{21}\text{Ne}/^{20}\text{Ne}_{\text{air}}$ is carried out using a high resolution mass spectrometer, the value reported here (0.002959 ± 0.000004) should be considered as the best estimate for the primary international standard.

4.4. Implications for Ne isotope determinations

4.4.1. Accuracy of Ne isotope data

We have demonstrated that the $^{20}\text{NeH}^+$ contribution at $m/z = 21$ varies between 0.4% and 2.3%, broadly consistent with previous studies (Honda et al., 2015; Wielandt and Storey, 2019). Further, $^{20}\text{NeH}^+$ production is strongly governed by source parameters. The NeH^+ contribution at $m/z = 21$ is a similar order as the reproducibility of $^{21}\text{Ne}/^{20}\text{Ne}$ ratio measurements of multiple air standards in the majority of operating instruments (0.5–1%; Ballentine et al. (1991); Györe et al. (2015)).

The NeH -corrected measurements of $^{21}\text{Ne}/^{20}\text{Ne}$ ratios in air standards will produce mass fractionation factors that are different from those calculated without the correction. NeH -uncorrected $^{21}\text{Ne}/^{20}\text{Ne}$ ratios of unknowns will be inaccurate only if the NeH correction was different to the relevant air calibration measurements. Typically, the measured Ne signal from minerals and rocks is significantly less than the amount of air-Ne used for mass discrimination and sensitivity determinations (e.g. Ritter et al., 2018). A 10-fold decrease in Ne abundance significantly affects the NeH^+ correction, resulting in an increased $^{21}\text{Ne}/^{20}\text{Ne}$ of up to 0.7% at 70 eV, and 0.15% for 110 eV (Fig. 3B) (see differences in correction techniques outlined in Table 4). Similar effects are noted for modest changes in the H_2^+ ; for instance, 1% increase results in a 0.3% increase in $^{21}\text{Ne}/^{20}\text{Ne}$ at 60 eV (Fig. 3A). Getter pumps attached to mass spectrometer source blocks go some way to minimising background hydrogen levels. The extent to which they maintain a constant level is unclear as the level of H_2^+ is rarely reported in published work, consequently it is difficult to assess the extent to which it has affected published Ne isotope data. Experience from the workhorse MAP 215–50 instrument in the SUERC laboratory shows that H_2^+ signal varies $\pm 5\%$ over several days. This could result in a 1% variation in $^{21}\text{Ne}/^{20}\text{Ne}$ ratio (Fig. 3A).

The combined effect of lower Ne^+ and higher H_2^+ in the analysis of unknowns compared to air standards means that $^{21}\text{Ne}/^{20}\text{Ne}$ ratios may be overestimated beyond the quoted 1σ uncertainty. This has implications for studies where accurate Ne isotope ratio determinations are important. An obvious case is the determination of Ne isotope composition of the terrestrial mantle. Accurate $^{21}\text{Ne}/^{20}\text{Ne}$ ratios are essential for distinguishing lithosphere from asthenosphere mantle sources (Gautheron et al., 2005;

Jalowitzki et al., 2016) and, in the case of intra-plate basaltic volcanism, for distinguishing a deep, relatively undegassed mantle source from the convecting upper mantle (e.g. Trierloff et al., 2000).

4.4.2. Improving the precision of Ne isotope analysis

We have shown here that state-of-the-art low resolution (<3300) noble gas mass spectrometers are now capable of Ne isotope ratio precision (± 0.1 – 0.2%), that is significantly less than the potential contribution of $^{20}\text{NeH}^+$ at $m/z = 21$. In order to ensure the veracity of Ne isotope determinations, we suggest that $^{20}\text{NeH}^+$ be determined and corrections made for analyses by low resolution mass spectrometers. The uncertainty reported here was obtained from analysis of aliquots of $2.2 \times 10^{-8} \text{ cm}^3 \text{ STP } ^{20}\text{Ne}$ measured using Faraday detectors in multi-collection mode. This is ~ 100 times more than routinely used on the SUERC MAP 215–50 mass spectrometer ($8 \times 10^{-10} \text{ cm}^3 \text{ STP } ^{20}\text{Ne}$, average reproducibility $\sim 1\%$). Neon isotope analysis of $3.38 \times 10^{-10} \text{ cm}^3 ^{20}\text{Ne}$ on the ARGUS VI mass spectrometer yields $^{21}\text{Ne}/^{20}\text{Ne}$ reproducibility of $\pm 3\%$ ($n = 10$). Assuming linear relationship between relative error and concentration this represents nearly an order of magnitude improvement in the uncertainty compared to the MAP 215–50 mass spectrometer. Given that the reproducibility of the standard is the governing factor for uncertainty of unknowns, we suggest that low volume, high precision low resolution mass spectrometer such as the Thermo Fisher ARGUS VI is capable of producing high precision Ne analysis, suitable for most geoscience applications.

The improved precision of isotope ratio determinations combined with the lower uncertainty of air $^{21}\text{Ne}/^{20}\text{Ne}$ has implications for studies that require the calculation of the absolute amount of non-atmospheric ^{21}Ne ($^{21}\text{Ne}^*$), such as cosmogenic exposure dating (Codilean et al., 2008; Ritter et al., 2018) and (U-Th)/Ne geochronology (Gautheron et al., 2006).

At its simplest the non-atmospheric ^{21}Ne concentration is calculated from:

$$^{21}\text{Ne}^* = S_{21} ^{21}\text{Ne}_{meas} \left[\frac{\left(\frac{^{21}\text{Ne}}{^{20}\text{Ne}} \right)_{meas} - \left(\frac{^{21}\text{Ne}}{^{20}\text{Ne}} \right)_{air}}{\left(\frac{^{21}\text{Ne}}{^{20}\text{Ne}} \right)_{meas}} \right] \quad (2)$$

where S_{21} refers to the sensitivity for ^{21}Ne and the subscript *meas* refers to measured. For a hypothetical sample with $^{21}\text{Ne}/^{20}\text{Ne}$ that is twice the air value, the uncertainty in the $^{21}\text{Ne}^*$ concentration using the Eberhardt et al. (1965) air value ($\pm 0.74\%$) and typical isotope ratio reproducibility of last-generation instruments (e.g. MAP 215–50 or VG5400; $\pm 1\%$), is approximately 3.5 times higher than if determined on state-of-the-art instrument ($\pm 0.3\%$ for the ARGUS VI in this study) and new air value ($\pm 0.14\%$; this work). These improvements translate directly to the uncertainty of cosmogenic ^{21}Ne exposure ages and (U-Th)/ ^{21}Ne cooling ages. Systematic reporting of Ne isotope ratio uncertainties requires that the external reproducibility of standards is used, rather than within-run uncertainties.

5. CONCLUSIONS

A Thermo Fisher ARGUS VI noble gas mass spectrometer has been used for high precision multi-collection determination of Ne isotopes in air. The method fully accounts for the formation of $^{20}\text{NeH}^+$ via the measurement of $^{22}\text{NeH}^+$. The production of $^{20}\text{NeH}^+$ is strongly dependent on source tuning, the level of Ne^+ and residual H_2^+ in the mass spectrometer during analysis. Consequently, it cannot be assumed that $^{22}\text{Ne}/^{20}\text{Ne} = ^{22}\text{NeH}^+/^{20}\text{NeH}^+$. Ne^+ - NeH^+ calibration curves for constant hydrogen levels are required to avoid over-correction of $^{20}\text{NeH}^+$, which we found may be up to 0.7%. Hydride-corrected Ne isotope data from multiple aliquots of air define a single mass fractionation line that produces $^{21}\text{Ne}/^{20}\text{Ne}_{air} = 0.002959 \pm 0.000004$ (0.14%, 1σ) at $^{22}\text{Ne}/^{20}\text{Ne}_{air} = 0.102$. This overlaps the commonly-used value of Eberhardt et al. (1965) and the recent redetermination by Wielandt and Storey (2019). The uncertainties in the latter study are underestimated and we recommend that the new, albeit less precise, value is used because the effect of pressure is taken into account. The uncertainty of the mass fractionation line in the $^{22}\text{Ne}/^{20}\text{Ne}$ vs. $^{21}\text{Ne}/^{20}\text{Ne}$ space is now governed by that of $^{22}\text{Ne}/^{20}\text{Ne}$, thus it is time for absolute $^{22}\text{Ne}/^{20}\text{Ne}$ redeterminations of air by measurement of manufactured Ne standards with accurately known ratios (gravimetry) and/or by theoretical means following the work of Valkiers et al. (2008). Ensuring the quality of Ne isotope determinations requires that $^{20}\text{NeH}^+$ is measured and corrected-for in Ne isotope analysis using low resolution mass spectrometers.

ACKNOWLEDGEMENTS

This work was funded by SUERC. We thank Dr Lorraine Ruzié-Hamilton for help developing this project. Dr Darren Mark and Dr Ángel Rodés, are thanked for their help in statistics. We thank Tom Darrah, Ken Farley and an anonymous reviewer for their constructive comments that helped improving presentation.

APPENDIX A. SUPPLEMENTARY MATERIAL

Supplementary data to this article can be found online at <https://doi.org/10.1016/j.gca.2019.07.059>.

REFERENCES

- Bai X., Qiu H., Liu W. and Mei L. (2018) Automatic $^{40}\text{Ar}/^{39}\text{Ar}$ dating techniques using multicollector ARGUS VI noble gas mass spectrometer with self-made peripheral apparatus. *J. Earth Sci.* **29**, 408–415.
- Balco G. and Shuster D. L. (2009) Production rate of cosmogenic Ne in quartz estimated from Be, Al, and Ne concentrations in slowly eroding Antarctic bedrock surfaces. *Earth. Planet. Sci. Lett.* **281**, 48–58.
- Ballentine C. J., Marty B., Sherwood Lollar B. and Cassidy M. (2005) Neon isotopes constrain convection and volatile origin in the Earth's mantle. *Nature* **433**, 33–38.
- Ballentine C. J. and O'Nions R. K. (1991) The nature of mantle neon contributions to Vienna Basin hydrocarbon reservoirs. *Earth. Planet. Sci. Lett.* **113**, 553–567.

- Ballentine C. J., O’Nions R. K., Oxburgh E. R., Horvath F. and Deak J. (1991) Rare gas constraints on hydrocarbon accumulation, crustal degassing and groundwater flow in the Pannonian Basin. *Earth. Planet. Sci. Lett.* **105**, 229–246.
- Black D. C. (1972) On the origins of trapped helium, neon and argon isotopic variations in meteorites-I. Gas-rich meteorites, lunar soil and breccia. *Geochim. Cosmochim. Acta* **36**, 347–375.
- Bottomley D. J., Ross J. D. and Clarke W. B. (1984) Helium and neon isotope geochemistry of some ground waters from the Canadian Precambrian Shield. *Geochim. Cosmochim. Acta* **48**, 1973–1985.
- Codilean A. T., Bishop P., Stuart F. M., Hoey T. B., Fabel D. and Freeman S. P. H. T. (2008) Single-grain cosmogenic Ne concentrations in fluvial sediments reveal spatially variable erosion rates. *Geology* **36**, 159–162.
- Colin A., Moreira M., Gautheron C. and Burnard P. (2015) Constraints on the noble gas composition of the deep mantle by bubble-by-bubble analysis of a volcanic glass sample from Iceland. *Chem. Geol.* **417**, 173–183.
- Eberhardt P., Eugster O. and Marti K. (1965) A redetermination of the isotopic composition of atmospheric neon. *Z. Naturforsch.* **20a**, 623–624.
- Gautheron C., Lassan-Got L. and Farley K. A. (2006) (U–Th) / Ne chronometry. *Earth. Planet. Sci. Lett.* **243**, 520–535.
- Gautheron C., Moreira M. and Allègre C. (2005) He, Ne and Ar composition of the European lithospheric mantle. *Chem. Geol.* **217**, 97–112.
- Györe D., Stuart F. M., Gilfillan S. M. V. and Waldron S. (2015) Tracing injected CO₂ in the Cranfield enhanced oil recovery field (MS, USA) using He, Ne and Ar isotopes. *Int. J. Greenh. Gas Con.* **42**, 554–561.
- Harrison D., Burnard P. and Turner G. (1999) Noble gas behaviour and composition in the mantle: constraints from the Iceland Plume. *Earth. Planet. Sci. Lett.* **171**, 199–207.
- Heber V. S., Wieler R., Baur H., Olinger C., Friedman T. A. and Burnett D. S. (2009) Noble gas composition of the solar wind as collected by the Genesis mission. *Geochim. Cosmochim. Acta* **73**, 7414–7432.
- Honda M., Zhang X., Phillips D., Hamilton D., Deerberg M. and Schwieters J. B. (2015) Redetermination of the Ne relative abundance of the atmosphere, using a high resolution, multi-collector noble gas mass spectrometer (HELIX-MC Plus). *Int. J. Mass spectrom.* **387**, 1–7.
- Jalowitzki T., Sumino H., Conceição R. V., Orihashi Y., Nagao K., Bertotto G. W., Balbinot E., Schilling M. E. and Gervasoni F. (2016) Noble gas composition of subcontinental lithospheric mantle: An extensively degassed reservoir beneath Southern Patagonia. *Earth. Planet. Sci. Lett.* **450**, 263–273.
- Kaul W., Lauterbach U. and Taubert R. (1961) Die Aufttrittspotentiale von HeH⁺, NeH⁺, AH⁺, KrH⁺, KrD⁺ und H₂⁺. *Z. Naturforsch.* **16a**, 624–625.
- King S. J. and Price S. D. (2008) Electron ionization of CO₂. *Int. J. Mass spectrom.* **272**, 154–164.
- Kirkup L. (2012) *Data Analysis for Physical Scientists, Featuring Excel*, 2nd Edition. Cambridge University Press.
- Ma Y. and Stuart F. M. (2018) The use of in-situ cosmogenic Ne in studies on long-term landscape development. *Acta Geochim.* **37**, 310–322.
- Man K. F., Smith A. C. H. and Harrison M. F. A. (1993) A measurement of the cross section for electron impact ionization of Ar²⁺, Kr²⁺ and Xe²⁺. *J. Phys. B: At Mol. Opt. Phys.* **26**, 1365–1378.
- Mark D. F., Stuart F. M. and de Podesta M. (2011) New high-precision measurements of the isotopic composition of atmospheric argon. *Geochim. Cosmochim. Acta* **75**, 7494–7501.
- Mishima K., Sumino H., Otono H., Yamada T. and Oide H. (2019) Accurate determination of the absolute ³He/⁴He ratio of a synthesized helium standard gas (Helium Standard of Japan, HESJ): toward revision of the atmospheric ³He/⁴He ratio. *Geochem. Geophys. Geosyst.* **19**, 3995–4005.
- Moran T. F. and Friedman L. (1963) Neon-hydrogen ion molecule reactions. *J. Chem. Phys.* **39**, 2491–2500.
- Moreira M., Kunz J. and Allègre C. (1998) Rare gas systematics in popping rock: isotopic and elemental compositions in the upper mantle. *Science* **279**, 1178–1181.
- Niedermann S., Graf T. and Marti K. (1993) Mass spectrometric identification of cosmic-ray-produced neon in terrestrial rocks with multiple neon components. *Geochim. Cosmochim. Acta* **118**, 65–73.
- Nier A. (1950) A redetermination of the relative abundances of the isotopes of neon, krypton, rubidium, xenon, and mercury. *Phys. Rev.* **79**, 450–454.
- Osawa T. (2004) A new correction technique for mass interferences by Ar⁺⁺ and CO₂⁺⁺ during isotope analysis of a small amount of Ne. *J. Mass Spectrometry Soc. Japan* **52**, 230–232.
- Poreda R. and di Brozolo F. R. (1984) Neon isotope variations in Mid-Atlantic Ridge basalts. *Earth. Planet. Sci. Lett.* **69**, 277–289.
- Ritter B., Binne S. A., Stuart F. M., Wennrich V. and Dunai T. J. (2018) Evidence for multiple Plio-Pleistocene lake episodes in the hyperarid Atacama Desert. *Quat. Geochronol.* **44**, 1–12.
- Ruzi-Hamilton L., Clay P. L., Burgess R., Joachim B., Ballentine C. J. and Turner G. (2016) Determination of halogen abundances in terrestrial and extraterrestrial samples by the analysis of noble gases produced by neutron irradiation. *Chem. Geol.* **437**, 77–87.
- Sessions A. L., Burgoyne T. W. and Hayes J. M. (2001) Determination of the H₃ factor in hydrogen isotope ratio monitoring mass spectrometry. *Anal. Chem.* **73**, 200–207.
- Smyth H. D. (1925) Primary and secondary products of ionization in hydrogen. *Phys. Rev.* **25**, 452–468.
- Trieloff M., Kunz J., Clague D. A., Harrison C. J. and Allègre C. J. (2000) The nature of pristin noble gases in mantle plumes. *Science* **288**, 1036–1038.
- Valkiers S., Schaefer F. and Bievre P. (1994) Near-absolute gas (isotope) mass spectrometry: isotope abundance (and atomic weight) determinations of neon, krypton, xenon and argon. In *Separation Technology* (ed. E. F. Vansant). Elsevier, pp. 965–968.
- Valkiers S., Varlam M., Berglund M., Taylor P., Gonfiantini R. and De Bièvre P. (2008) Absolute measurements of isotope amount ratios on gases. *Int. J. Mass spectrom.* **269**, 71–77.
- Walton J. R. and Cameron A. E. (1966) The isotopic composition of atmospheric neon. *Z. Naturforsch. A: Phys. Sci.* **21a**, 115–119.
- Wielandt D. and Storey M. (2019) A new high precision determination of the atmospheric Ne abundance. *J. Anal. At. Spectrom.* **34**, 535–549.
- Wieler R. (2002) Noble gases in the solar system. *Rev. Min. Geochem.* **47**, 21–70.